HHS Public Access

Author manuscript

Magn Reson Med. Author manuscript; available in PMC 2021 August 01.

Published in final edited form as:

Magn Reson Med. 2020 August ; 84(2): 634–645. doi:10.1002/mrm.28140.

T_1 measurement of bound water in cortical bone using 3D adiabatic inversion recovery ultrashort echo time (3D IR-UTE) Cones imaging

Tan Guo[1,2], **Yajun Ma**[2], **Saeed Jerban**[2], **Hyungseok Jang**[2], **Wei Zhao**[2], **Eric Y Chang**[3], **Min Chen**[1], **Graeme M Bydder**[2], **Jiang Du**[2]

[1]Department of Radiology, Beijing Hospital, Beijing, China

[2]Department of Radiology, University of California, San Diego, CA

[3]Research Service, VA San Diego Healthcare System, San Diego, CA

Abstract

Purpose: We describe the measurement of bound water T_1 (T_1^{BW}) of cortical bone in vitro and in vivo with a 3D adiabatic inversion recovery ultrashort echo time (IR-UTE) Cones sequence using a clinical 3T scanner.

Methods: A series IR-UTE data from six repetition times (TRs) with five inversion times (TIs) at each TR were acquired from 12 human tibial bone specimens, and data from four TRs with five TIs at each TR were acquired from the tibial midshafts of eight healthy volunteers. The pore water nulling point was calculated from exponential fitting of the inversion recovery curve at each TR. Bone specimens and volunteers were then scanned again with the calculated nulling point at each TR. T_1^{BW} was derived through exponential fitting of data from IR-UTE images acquired at different TRs using the calculated pore water nulling point for each TR.

Results: In vitro pore water nulling TIs were 141.3±11.6, 123.4±8.9, 101.3±6.2, 88.9±5.3, 74.8±4.2, and 59.2±3.9 ms for the six TRs of 500, 400, 300, 250, 200 and 150ms, respectively. In vivo pore water nulling TIs were 132.8±12.8, 110.3±10.0, 80.0±7.2, and 63.9±5.4 ms for the four TRs of 400, 300, 200 and 150 ms, respectively. Excellent exponential fitting was achieved for IR-UTE imaging of bound water with pore water nulled at each TR. The mean T_1^{BW} was 106.9±6.3 ms in vitro and 112.3±16.4 ms in vivo.

Conclusion: Using the 3D IR-UTE Cones with a variable TR/TI approach, T_1^{BW} of cortical bone was calculated after complete nulling of pore water signals.

Keywords

cortical bone; UTE; adiabatic inversion recovery; bound water; T_1 measurement

Corresponding Author Info: Jiang Du, Ph.D., Department of Radiology, University of California, San Diego, 200 West Arbor Drive, San Diego, CA 92103-8226, jiangdu@ucsd.edu, Phone: (619) 471-0519, Fax: (619) 471-0503.

INTRODUCTION

The primary constituents of bone are collagen type I, calcium phosphate in the form of hydroxyapatite, and water (1). The water, which makes up around 20% of the volume of bone is present, in different states: (i) as extracellular free water, referred to as “pore water”, which resides in the anatomical pores of cortical bone and which includes the vascular space within Haversian and Volkmann’s canals, as well as the lacuna-canalicular network (2, 3); (ii) as loosely bound water which is found on the surface of collagen fibrils and between collagen helping orient apatite crystals during biomineralization (4); (iii) as tightly bound water trapped by hydrophilic residues inside the collagen triple helix as water bridges (5), and (iv) as mineral lattice water found within the core of the bone’s apatite structure (6).

Water influences the mechanical behavior of bone and is a primary determinant of fracture resistance. Along with collagen, it confers ductility and plasticity to bone, and affects bone viscoelastic behavior (7). However, changes in water compartments in cortical bone may affect bone properties in different ways, such as an increase in hardness or stiffness, and a decrease in elastic moduli (8, 9). Bound and pore water in particular are believed to affect bone properties differently (10, 11); this may explain their different effects on strength and flexural modulus (12). Bound water appears to be more related to post-yield properties as it confers collagen ductility (13), whereas pore water is more related to porosity, and bone stiffness (14). Better characterization of water in different bone compartments may lead to improved understanding of bone mechanical properties may follow from.

Both bound and pore water in cortical bone have short or ultrashort apparent transverse relaxation times (T_2*s) (in the range of a few milliseconds for pore water and a few hundreds of microseconds for bound water (15)). As a result, cortical bone appears as a signal void when imaged using conventional clinical sequences which have echo times (TEs) of a few milliseconds, and are typically longer than the T_2*s of cortical bone components. However, this limitation can largely be overcome by the use of ultrashort echo time (UTE) sequences, which provide direct imaging of cortical bone by using a nominal TE of 8~32 μs(16-20).

While the UTE sequence allows simultaneous signal acquisition from both bound water and pore water components, it is important to distinguish the contributions of these two water compartments to the UTE-MRI signal when evaluating bone properties. MRI biomarkers of bound water have been shown to be positively correlated with both strength and toughness of hydrated bone, and may present useful clinical markers of fracture risk (5, 21). Bi-component fitting of UTE T_2* signal decay has been used to separate and evaluate bound and pore water compartments, and their T_2*s and relative fractions have been used as independent biomarkers of bone mechanical properties (22).

The T_1 values of cortical bone water may also serve as independent biomarkers of bone properties. For example, pore water T_1 (T_1^{PW}) shows a correlation with aging ($R^2 = 0.72$), as aged bone has increased cortical porosity with a longer T_1^{PW} (23). Though there is no literature supporting bound water T_1 (T_1^{BW}) being used as an independent biomarker of bone properties, it is required for direct measurement of bound water proton density, which

represents the bone collagenous matrix spatial distribution and potentially correlates with bone's viscoelastic properties (24, 25). (22)(26)Therefore, accurate measurement of T_1^{BW} is therefore needed for indirect assessment of bone organic matrix properties.

However, it is technically challenging to measure T_1^{BW}, due to its extremely short T_2*. Most available methods for T_1 mapping are only valid for long T_2 tissues, and are not directly applicable to cortical bone. Furthermore, it is important to selectively image only bound water in order to measure its T_1. With an adiabatic inversion recovery (IR) preparation pulse, pore water signal can be nulled with an appropriate combination of repetition time (TR) and inversion time (TI), leaving bound water signal to be selectively detected by subsequent UTE data acquisition (15, 27). T_1^{BW} can be calculated by modeling IR-UTE signal as a function of TR and TI. TI is a critical parameter in IR-UTE imaging of bound water. Inaccurate TI values may lead to significant pore water contamination and, consequently, inaccurate T_1^{BW} measurement (27). The aim of this study was to demonstrate the use of a 3D IR-UTE Cones technique to accurately measure the T_1^{BW} of cortical bone in vitro and in vivo using a clinical 3T scanner.

METHODS

Specimen Preparation

12 cortical bone specimens were harvested from freshly frozen cadaveric human tibial midshafts (66.8 ± 22.6 years old, four males, eight females), provided by a non-profit whole-body donation company (United Tissue Network, Phoenix, AZ). Cortical bone segments (30 mm in length) were cut from the anterior part of each tibial midshaft using a Delta ShopMaster band saw (Delta Machinery, Tennessee, USA). Bone marrow was removed with a scalpel. All bone specimens were immersed in phosphate-buffered saline (PBS) for four hours at room temperature before MRI scanning. The bone samples were placed in a 30 ml plastic syringe filled with Fomblin (Fomblin, Ausimont, Thorofare, NJ) to minimize dehydration and susceptibility artifacts at air-tissue interfaces.

Pulse Sequences

The 3D IR-UTE Cones sequence combined a basic 3D Cones UTE sequence with an adiabatic IR preparation pulse (Silver-Hoult pulse, duration = 8.64 ms, bandwidth = 1.15 KHz, maximum B1 = 12 μT) (28, 29). To improve the acquisition efficiency, a series of spokes (N_{sp}) were acquired after each IR pulse (Figure 1A). The time interval between two adjacent spokes was defined as τ. For each spoke, a short rectangular pulse (50 μs) was employed for non-selective signal excitation with a flip angle (FA) of 20° (Figure 1B) followed by 3D spiral sampling with dual-echo acquisition (TEs of 32 μs and 2.5 ms) (Figure 1C). The 3D Cones sequence used an unique k-space sampling trajectory that sampled data along evenly spaced paths on cone surfaces (30). The sampled data started from the center of k-space and twisted outward, with the data acquisition starting as soon as possible after the RF excitation. Both RF and gradient spoiling were used to crush residual transverse magnetization after each data acquisition.

Pore water in cortical bone has a relatively long T_2* (typically ~2 ms or longer), and its longitudinal magnetization is partially inverted by the adiabatic IR pulse. The partially inverted longitudinal magnetization of pore water then recovers based on its T_1 relaxation (15, 31). On the other hand, bound water has an extremely short T_2* (typically ~0.3 ms), and its longitudinal magnetization is largely saturated (not inverted), since its T_2* is much shorter than the duration of the adiabatic IR pulse (i.e., 0.3 ms vs. 6 ms) (17). During the recovery of the longitudinal magnetizations of pore and bound water, signal from bound water can be preferentially acquired when data acquisition starts at or near the signal nulling point for pore water (Figure 1D). As a result, T_1^{BW} can be calculated using the variable TR/TI approach as described below.

Fitting Model

The steady-state IR-UTE signal following an adiabatic IR pulse can be written as:

$$S^{IR-UTE} = S_0^{IR-UTE} \times [1 + (Q-1) \times e^{-TI/T_1} - Q \times e^{-TR/T_1}] / (1 - Q \times cos\theta \times e^{-TR/T_1}), \quad [1]$$

where S_0^{IR-UTE} is the IR-UTE signal of cortical bone in the steady state, Q is the inversion fraction of longitudinal magnetization following the adiabatic IR pulse (with −1 meaning full inversion, and 0 meaning full saturation), and θ is the flip angle. If we consider that bound water and pore water in cortical bone have different T_1s and T_2s/T_2*s, and thus different Q values, Eq. [1] can be rewritten as:

$$\begin{aligned} S^{IR-UTE} &= S_{BW}^{IR-UTE} + S_{PW}^{IR-UTE} \\ &= S_{0,BW}^{IR-UTE} \times [1 + (Q_{BW}-1) \times e^{-TI/T_1^{BW}} - Q_{BW} \times e^{-TR/T_1^{BW}}] / (1 - Q_{BW} \times cos\theta \times e^{-TR/T_1^{BW}}) + S_{0,PW}^{IR-UTE} \times [1 + (Q_{PW}-1) \times e^{-TI/T_1^{PW}} - Q_{PW} \times e^{-TR/T_1^{PW}}] / (1 - Q_{PW} \times cos\theta \times e^{-TR/T_1^{PW}}) \end{aligned} \quad [2]$$

where S_{BW}^{IR-UTE} and S_{PW}^{IR-UTE} are the IR-UTE signals of bound water and pore water, respectively, and Q_{BW} and Q_{PW} are the corresponding inversion fractions of bound water and pore water, respectively, following the adiabatic IR pulse. The extremely short T_2/T_2* (~ 0.3 ms) of bound water and 8.64 ms duration of the adiabatic IR pulse yield a Q_{BW} value of near zero (< 0.05). Bloch equation simulation suggests near complete saturation of signal for the bound water component (2,10,11). On the other hand, pore water has a relatively short T_2* (a few milliseconds), but much longer T_2 (up to 1000 ms or longer), yielding a Q_{PW} value of near −1, or near full inversion.

When a relatively long TE is used, the bound water signal decays to zero and only the signal from pore water is detected. Therefore, the behavior of pore water signal with TI following an adiabatic IR pulse can be depicted by Eq. [3]:

$$S^{PW}(\mathrm{TR}, \mathrm{TE} = 2.5\mathrm{ms}) = S_0^{PW} \times [1 + (Q_{PW} - 1) \times e^{-TI / T_1^{PW}} - Q_{PW} \times e^{-TR / T_1^{PW}}] / (1 - Q_{PW} \times cos\theta \times e^{-TR / T_1^{PW}}) + noise, \quad [3]$$

where S_0^{PW} is the pore water signal of cortical bone in steady state acquired at a TE of 2.5 ms.

The pore water signal intensity after the adiabatic IR pulse depends on the value of TI. When S^{PW}(TR, TE = 2.5ms) in Eq. [3] is equal to the background noise, the nulling point of pore water can be derived from the simplified equation:

$$TI_{null} = -\ln\frac{Q_{PW} \times e^{-TR / T_1^{PW}} - 1}{Q_{PW} - 1} \times T_1^{PW}, \quad [4]$$

where TI_{null} is the pore water nulling point. T_1^{PW} can be estimated from the observed signal at different TIs from Eq. [3]. Using Eq. [3] and Eq. [4], TI_{null} can be estimated.

For IR-UTE images acquired at TI_{null}, pore water signal is largely suppressed and only bound water contributes to the total signal. T_1^{BW} can then be derived from the following simplified equation:

$$S^{BW}(\mathrm{TR}, \mathrm{TE} = 32\mu\mathrm{s}) = S_0^{BW} \times \left(1 - e^{-TI_{null} / T_1^{BW}}\right), \quad [5]$$

where S^{BW}(TR, TE = 32 μs) represents the signal intensity of bound water for a particular TR using a TE of 32 μs. T_1^{BW} can be measured with exponential fitting of IR-UTE images acquired at different TRs, provided that an appropriate TI is chosen to null the pore water signal at each TR. Although TR is not shown explicitly in Eq. [5], the TI for nulling depends on TR (32).

Determination of TI

It is critical to accurately estimate the nulling time for pore water in order to achieve selective imaging of bound water, and, consequently, an accurate estimation of T_1^{BW}. In this study, we propose to acquire dual-echo IR-UTE images with a series of TIs for each TR. Then, the best nulling point will be determined by fitting the IR-UTE signal vs. TI for the second echo, where only signal from pore water is detected (bound water signal decays to the noise level with a TE of 2.5 ms). The same process is repeated so that the corresponding nulling points are accurately measured. A final set of IR-UTE images is acquired with the optimal TR/TI combination based on the fitting results. T_1^{BW} is then calculated by fitting bound water signal vs. TI based on Eq. [5].

In vitro T_1^{BW} measurement

Cortical bone samples were scanned with a homemade 30 ml birdcage coil on a clinical 3T scanner (MR750, GE Healthcare, Milwaukee, WI). A series of 3D IR-UTE Cones images with multiple TRs and TIs were acquired, as shown in Table 1. A total of six TRs (500, 400,

300, 250, 200, 150 ms) were chosen with multiple TIs at each TR to cover the likely nulling points of pore water, ranging from the minimum to the maximum TI available for each TR. TIs were distributed non-uniformly, with more TIs around the nulling points and fewer TIs away from the nulling points. To speed up this technique, nulling points were also derived from five TIs for each TR, and were compared with those from multiple TIs. Each 3D IR-UTE Cones acquisition was performed with dual echoes (TE = 32 μs/2.5 ms), FA = 20°, pulse length = 50 μs, bandwidth (BW) = 125 kHz, N_{sp} = 5, τ = 8.3 ms, field of view (FOV) = 8 cm, slice thickness = 4 mm, reconstruction matrix = 128×128, number of slices = 20. After calculating the pore water nulling point for each TR, the bone samples were scanned again using the same 3D IR-UTE Cones imaging protocol, but six different TR/TI combinations with the fitted pore water nulling point chosen for each TR.

In vivo T_1^{BW} measurement

The 3D IR-UTE Cones sequence was applied to the tibial midshafts of eight healthy volunteers (mean age = 40.9 ± 14.3 years old, seven males, one female) for determination of pore water nulling points and measurement of T_1^{BW} in vivo. The in vivo studies were performed with Institutional Review Board approval and written informed consent was obtained from each participant. A 3-inch surface coil was used for signal reception and the body coil was used for signal excitation. The surface coil was attached next to the skin near the tibial midshaft. The center of the excitation slab was positioned at ~38% of the tibia length measured from the medial malleolus (an easily identifiable anatomic landmark). Oblique axial imaging was performed with the slices perpendicular to the tibia to minimize partial volume effects. Four TRs (400, 300, 200, 150 ms) with five TIs at each TR were used to cover the likely nulling points of pore water for the tibial midshaft of volunteers, as shown in Table 1. 3D IR-UTE Cones acquisitions were performed with dual echo (TE = 32 μs/2.5 ms), FA = 20°, pulse length = 50 μs, BW = 125 kHz, N_{sp} = 5, τ = 8.3 ms, FOV = 10 cm, slice thickness = 6 mm, reconstruction matrix = 128×128, number of slices = 10. The optimal TI was calculated for each TR according to Eq. [4]. The volunteers were scanned again using the same 3D IR-UTE Cones imaging protocol, but with the calculated pore water nulling TI for each TR. The total in vivo scan time was approximately 60 minutes.

MRI data analysis

The analysis algorithm was written in MATLAB (The MathWorks, Natick, Massachusetts) and was executed offline on the DICOM images obtained with the protocols described previously. For the specimen study, three regions of interest (ROIs) were placed in the center of each cortical bone fragment in three consecutive slices to avoid susceptibility effects near the bone interface and incorporation of any residual fat from bone marrow. For the volunteer study, three ROIs in three consecutive slices were placed anteriorly in the tibial cortex close to the surface coil for higher signal to noise ratio (SNR) measurements. The ROI positioning was performed on the image with a TE of 32 μs and at the mid TI for each TR series because of the relatively high signal and contrast seen in cortical bone. The ROI was then copied automatically to the corresponding site for all the images performed with other TIs at each TR. The TI for nulling pore water was calculated using Eq. [4]. Further, Eq. [5] was used for T_1^{BW} measurement, when IR-UTE Cones acquisitions were repeated using the pore water

nulling TI for each TR. The mean and standard deviation of T_1^{BW} were calculated for both the bone samples and the tibial midshafts of healthy volunteers.

Statistical Analysis

Agreement of the calculated pore water nulling points between five TIs fitting and multiple TI fitting for the specimens was assessed by the intraclass correlation coefficient (ICC). Agreement was categorized as follows: greater than 0.95, excellent; 0.95 – 0.85, strong; 0.85 – 0.70, good; 0.70 – 0.5, moderate; less than 0.5, poor. The student t test was used to compare the calculated T_1^{BW} values in vitro and in vivo. A p-value less than 0.05 was considered statistically significant. Statistical analyses were performed with SPSS (v19.0, SPSS Inc., Chicago, IL).

RESULTS

Figure 2 shows selected images of a tibial midshaft bone segment from a 38-year-old donor scanned using the dual-echo 3D IR-UTE Cones sequence with variable TRs and TIs, as well as curve fitting to determine pore water nulling points with multiple TIs and with five TIs. Images acquired at the calculated pore water nulling point for each TR show high SNRs for pure bound water with a TE of 32 μs (higher SNR for longer TR/TIs), with the pore water signal successfully nulled as confirmed by the near zero signal intensity on the second echo. Excellent fitting curves delineating the changing absolute value of pore water signal during recovery were derived from fitting multiple TIs, as well as from five TI point fitting. Table 2 shows results from fitting with different TIs. This shows excellent ICCs in fitting the pore water nulling point with all data, and with only five TIs for each TR.

Figure 3 shows the trend change in signal intensities of the first echo and the second echo of 3D IR-UTE Cones images along with the increase of TIs for a particular TR. For each TI, the total signals acquired with a TE of 32 μs include contributions from both bound water and part of the unsuppressed pore water. When the selected TI was close to the pore water nulling point, bound water made the main contribution to the UTE signal. As TI increased, the longitudinal magnetization of pore water increased from a negative value to a positive value, and contributed to the final UTE signal. The signal contribution from pore water in 3D IR-UTE Cones images with the second TE of 2.5 ms was higher when the selected TI was near either the lower or the upper limit of the TI range; however, the longitudinal magnetization was in the opposite direction in these two situations, namely negative for the former and positive for the latter. When the selected TI was close to the nulling point, the signal from pore water was almost completely suppressed. Dual-echo 3D IR-UTE Cones images acquired at the pore water nulling point for each TR, as well as the T_1^{BW} fitting curve, are shown in Figure 4. Bound water images were obtained with high SNR, and the bound water signal increased with longer TRs. The mean TIs for pore water nulling were 141.3 ± 11.6, 123.4 ± 8.9, 101.3 ± 6.2, 88.9 ± 5.3, 74.8 ± 4.2, and 59.2 ± 3.9 ms for TRs of 500, 400, 300, 200 and 150 ms, respectively, in the specimen group, and the average T_1^{BW} for the sample group was 106.9 ± 6.3 ms.

Figure 5 shows fitting of pore water nulling point and T_1^{BW} for the tibial midshaft in the volunteers. The total signal from cortical bone at a TE of 32 μs increased with TI. The signal

trends of surrounding muscle as well as subcutaneous and bone marrow fat at a TE of 32 μs were similar to their trends at a TE of 2.5 ms. The adiabatic IR pulse inverted the longitudinal magnetization of pore water, while also inverting the longitudinal magnetization of fat and muscle. The signal intensities of the surrounding muscle and fat reached their minimum values with a TR of 400 ms and TIs of 160 ms and 110 ms, respectively. Excellent curve fitting was achieved at each TR, allowing accurate estimation of the pore water nulling point. When the fitted pore water nulling point was used for each 3D IR-UTE Cones data acquisition, pore water signal was completely nulled, allowing selective imaging of bound water whose signal intensity increased with TR, as shown in Figure 6. Excellent exponential fitting was achieved for bound water signal to optimize TI.

The mean pore water nulling TIs for volunteers were 132.8 ± 12.8, 110.3 ± 10.0, 80.0 ± 7.2, and 63.9 ± 5.4 ms for TRs of 400, 300, 200 and 150 ms, respectively. The average T_1^{BW} for the in vivo group was 112.3 ± 16.4 ms. There were no significant differences of cortical bone bound water T_1 values ($p = 0.3177$) between the in vivo and in vitro groups (Fig 7). However, we did observe a trend for T_1^{BW} which was higher in the in vivo group compared to the in vitro group.

DISCUSSION

UTE-MRI, with its ability to image tissues with extremely rapid transverse relaxation, has been successfully employed for cortical bone imaging in earlier studies (15, 27, 29, 31, 33). In this study, we showed the feasibility of employing the 3D IR-UTE Cones sequence to assess T_1^{BW} in vitro and in vivo. To achieve this goal, T_1^{BW} fitting was performed on pure bound water images acquired at different TRs, obtained after complete suppression of pore water signals using a series of accurately calculated pore water nulling times.

Over the past decade, UTE-MRI has been used to investigate correlations between different water compartments and the mechanical properties of cortical bone. Greater concentration of bound water is associated with higher peak stress, yield stress, and elastic toughness; however, pore water concentration is negatively correlated with these mechanical properties (12). Accurate discrimination between the signal from bound water and that from pore water in UTE-MRI requires a precise estimation of T_1^{BW} and T_1^{PW}. For direct bound water proton density measurement, T_1^{BW} is required in addition to the IR-UTE signal ratio between bone and an external water phantom (e.g., 20% H_2O plus 80% D_2O) (24, 25, 34, 35). Accurate assessment of T_1^{BW} is challenging because of its extremely short T_2* and the resultant contamination from longer T_2* tissues and fluids, particularly pore water. For accurate T_1^{BW} measurement, it is crucial to selectively image bound water to minimize pore water contamination.

The 3D IR-UTE Cones sequence is able to provide a high SNR for selective bound water imaging. Specifically, the adiabatic IR pulse inverts the longitudinal magnetizations of long T_2* signal components (i.e., muscle, fat and pore water), while the longitudinal magnetization of bound water is largely saturated because of its extremely short T_2*. After the IR pulse, the longitudinal magnetizations of the two water compartments experience different T_1 relaxations. During the inversion time, the saturated longitudinal magnetization

of bound water recovers from zero to positive, while the inverted longitudinal magnetization of pore water recovers from negative to zero (the nulling point), and then to positive. At the nulling point, pore water magnetization reaches zero which results in a dominant bound water signal. The calculation of pore water nulling point for each TR is based on the measured IR-UTE signal intensities and the corresponding TIs for the second echo, as shown in Eq. [4].

Only a limited number of studies have focused on T_1^{BW} measurement (15, 23, 27, 36, 37). Abbasi-Rad et al. (23) reported a mean T_1^{BW} of 162 ± 30 ms for tibial cortical bone in 40 healthy women (26 to 79 years old) at 3T. A series of equations derived from the Bloch equations was used to characterize the different water compartments, for which bound and pore water T_2* were unknown. They used a bound water T_2* of 0.33 ms and a pore water T_2* of 2.46 ms as constants extracted from the literature to calculate bound and pore water T_1s. Although their study benefited from a simple method and short acquisition time, the accuracy of T_1 measurements of bound and pore water may be affected by errors associated with the use of only two TRs and with variations in pore water T_2*s between cortical bone layers, individuals, and disease status (38, 39). Marcon et al. (36) reported a mean T_1^{BW} of 213 ± 95 ms (range 75 to 349 ms) for cortical bone of the femoral diaphysis in six mice at 4.7T. Bi-component exponential fitting was used to calculate bound and pore water T_1s. They reported very low fitting error values (0.016 ± 0.007); nevertheless, the range of T_1^{BW} was quite wide across the animals, and the standard deviation of T_1^{BW} was substantially higher than that in previous studies (15).

Horch et al. (15) reported a T_1^{BW} of 357 ± 10 ms for cortical bone samples of human femurs using IR Carr-Purcell-Meiboom-Gill (CPMG) sequences and fitting with a 2D T_1-T_2 spectrum at 4.7T. Chen et al. (27) reported a mean T_1^{BW} of 134 ± 11 ms for tibial midshaft of health volunteers at 3T, where TIs were selected based on the researchers' experience. Seifert et al. (37) reported a mean T_1^{BW} of 145 ± 25 ms for samples of human tibial midshaft at 3T, for which the TI was stepped from 10 to 270 ms at TR = 300 ms. Among these TIs, the one leading to the minimum signal intensity of pore water was selected as pore water nulling point. All these studies were based on the adiabatic IR scheme, creating a predominantly bound water image with most of the pore water signal suppressed. These approaches are similar to ours, except that our technique makes provision for more complete suppression of pore water and thus more selective imaging of bound water by using an accurately assessed pore water nulling point at each TR.

The pore water nulling point depends on the selected TR. The longer the selected TR, the longer the corresponding TI to achieve complete pore water nulling. When using a longer TR, the accuracy of the nulling point selection is more critical for suppressing pore water signal, as the nulling points for long TRs only cover tissues or fluids with a relatively narrow range of T_1s and vice versa, as shown in Figure 6B. For a longer TR (e.g., 300 or 400 ms), the pore water signal is nulled at its nulling point, whereas the signals from fat and muscle remain quite high. For a shorter TR (e.g., 150 or 200 ms), the adiabatic IR pulse provides excellent suppression of tissues with a broad range of T_1s (e.g., pore water, fat and muscle) by using a TI near the pore water nulling time. A slight deviation from the pore water nulling point may result in significant pore water signal contamination with a longer TR, but

much reduced pore water signal contamination with a shorter TR. Accurately calculated pore water nulling times effectively limit the contamination of pore water signal with ether longer or shorter TRs.

The bone specimen study suggests that a smaller number of TIs (e.g., five TIs) may provide accurate estimation of the optimal pore water nulling point. This approach helps reduce the total scan time compared with the multiple TI approach. The calculated pore water nulling points in cortical bone samples with the five TI approach were comparable with the results from the multiple TI approach. For further acceleration of the acquisition, five spokes were acquired after each IR pulse (28). Such accelerated acquisitions facilitate the translation of the technique to clinical studies. However, further development is needed as the total scan time is still long.

The T_1^{BW} values in our study were slightly shorter than the values reported by Chen et al. and Seifert et al. (27, 37). This is likely due to the precise calculation of the pore water nulling points at different TRs and reduced contamination of pore water signal. Both ex vivo and in vivo measured bound water T_1s of cortical bone in our study showed narrow variations, which is consistent with most previous studies (15, 27, 37). Though no significant difference was derived, a trend of higher bound water T_1 in vivo than that of specimens was observed. This might be explained by the higher temperature in the body compared with the room temperature of specimens. A recent study of Han et al. investigated the temperature dependence of T_1 in cortical bone at 3T using a varying flip angle approach and found that a linear relationship with T_1 which increased from 120 ms at 25.1℃ to 155 ms at 70.1℃ (40).

Pore water resides in the space of pores such as Haversian canals (typical diameter > 30 μm), lacunae (typical diameter, approximately 10 μm), and canalicular systems (typical diameter, approximately 0.5 mm) (5, 11, 23). The T_1^{PW} is related to the surface-to-volume ratio of the pores harboring them according to the surface relaxation mechanism(41). The different scales of pores may potentially result in multi-exponential pore water T_1 and T_2 relaxation, leading to pore water contamination due to incomplete nulling of multiple pore water components with the use of a single TI. Multiexponential T_2 spectroscopy of human cortical bone has revealed a broad distribution of long-lived T_2 components of pore water spanning 1 ms to 1000 ms (42). However, the majority of bone water exists in the form of bound water, and accounts for ~80% of the water in normal bone (43). In IR-UTE imaging with data acquired at TI_{null}, the residual pore water signal is likely to be very small. Nevertheless, double adiabatic IR or a train of adiabatic IR pulses may help improve the suppression of pore water with a range of T1s (44, 45), and so increase the accuracy of T_1^{BW} measurement.

In conclusion, we have demonstrated that the pore water nulling points of cortical bone can be accurately calculated by fitting the IR curves of dual echo 3D IR-UTE Cones data acquired with different TRs and TIs. Robust calculation of cortical bond bound water T_1 was feasible using a variable TR/TI approach with optimal pore water nulling at each TR.

ACKNOWLEDGEMENTS

The authors acknowledge grant support from NIH (2R01 AR062581, 1R01 NS092650, and 1R01 AR075825) and the National Natural Science Foundation of China (81801673).

REFERENCES

1. Mueller KH, Trias A, Ray RD. Bone density and compositon. Age-related and pathological changes in water and mineral content. J Bone Joint Surg Am. 1966; 48:140–148. [PubMed: 5902798]
2. Dong P, Haupert S, Hesse B, et al. 3D osteocyte lacunar morphometric properties and distributions in human femoral cortical bone using synchrotron radiation micro-CT images. Bone. 2014; 60:172–185. [PubMed: 24334189]
3. Robinson RA. Bone tissue: composition and function. Johns Hopkins Med J. 1979; 145:10–24. [PubMed: 376922]
4. Wang Y, Von Euw S, Fernandes FM, et al. Water-mediated structuring of bone apatite. Nat Mater. 2013; 12:1144–1153. [PubMed: 24193662]
5. Granke M, Does MD, Nyman JS. The role of water compartments in the material properties of cortical bone. Calcif Tissue Int. 2015; 97:292–307. [PubMed: 25783011]
6. Davies E, Muller KH, Wong WC, et al. Citrate bridges between mineral platelets in bone. Proc Natl Acad Sci U S A. 2014; 111:E1354–1363. [PubMed: 24706850]
7. Yamashita J, Li X, Furman BR, Rawls HR, Wang X, Agrawal CM. Collagen and bone viscoelasticity: a dynamic mechanical analysis. J Biomed Mater Res. 2002; 63:31–36. [PubMed: 11787026]
8. Faingold A, Cohen SR, Shahar R, Weiner S, Rapoport L, Wagner HD. The effect of hydration on mechanical anisotropy, topography and fibril organization of the osteonal lamellae. J Biomech. 2014; 47:367–372. [PubMed: 24332267]
9. Hengsberger S, Kulik A, Zysset P. Nanoindentation discriminates the elastic properties of individual human bone lamellae under dry and physiological conditions. Bone. 2002; 30:178–184. [PubMed: 11792582]
10. Burghardt AJ, Kazakia GJ, Ramachandran S, Link TM, Majumdar S. Age- and gender-related differences in the geometric properties and biomechanical significance of intracortical porosity in the distal radius and tibia. J Bone Miner Res. 2010; 25:983–993. [PubMed: 19888900]
11. Nyman JS, Ni Q, Nicolella DP, Wang X. Measurements of mobile and bound water by nuclear magnetic resonance correlate with mechanical properties of bone. Bone. 2008; 42:193–199. [PubMed: 17964874]
12. Horch RA, Gochberg DF, Nyman JS, Does MD. Non-invasive predictors of human cortical bone mechanical properties: T(2)-discriminated H NMR compared with high resolution X-ray. PLoS One. 2011; 6:e16359. [PubMed: 21283693]
13. Nyman JS, Roy A, Shen X, Acuna RL, Tyler JH, Wang X. The influence of water removal on the strength and toughness of cortical bone. J Biomech. 2006; 39:931–938. [PubMed: 16488231]
14. Granke M, Grimal Q, Saied A, Nauleau P, Peyrin F, Laugier P. Change in porosity is the major determinant of the variation of cortical bone elasticity at the millimeter scale in aged women. Bone. 2011; 49:1020–1026. [PubMed: 21855669]
15. Horch RA, Gochberg DF, Nyman JS, Does MD. Clinically compatible MRI strategies for discriminating bound and pore water in cortical bone. Magn Reson Med. 2012; 68:1774–1784. [PubMed: 22294340]
16. Gatehouse PD, Bydder GM. Magnetic resonance imaging of short T2 components in tissue. Clin Radiol. 2003; 58:1–19. [PubMed: 12565203]
17. Larson PE, Conolly SM, Pauly JM, Nishimura DG. Using adiabatic inversion pulses for long-T2 suppression in ultrashort echo time (UTE) imaging. Magn Reson Med. 2007; 58:952–961. [PubMed: 17969119]
18. Ma YJ, West J, Nazaran A, et al. Feasibility of using an inversion-recovery ultrashort echo time (UTE) sequence for quantification of glenoid bone loss. Skeletal Radiol. 2018; 47:973–980. [PubMed: 29396694]

19. Reichert IL, Robson MD, Gatehouse PD, et al. Magnetic resonance imaging of cortical bone with ultrashort TE pulse sequences. Magn Reson Imaging. 2005; 23:611–618. [PubMed: 16051035]
20. Techawiboonwong A, Song HK, Leonard MB, Wehrli FW. Cortical bone water: in vivo quantification with ultrashort echo-time MR imaging. Radiology. 2008; 248:824–833. [PubMed: 18632530]
21. Ma YJ, Chen Y, Li L, et al. Trabecular bone imaging using a 3D adiabatic inversion recovery prepared ultrashort TE Cones sequence at 3T. Magn Reson Med. 2019, 10.1002/mrm.28027
22. Bae WC, Chen PC, Chung CB, Masuda K, D'Lima D, Du J. Quantitative ultrashort echo time (UTE) MRI of human cortical bone: correlation with porosity and biomechanical properties. J Bone Miner Res. 2012; 27:848–857. [PubMed: 22190232]
23. Abbasi-Rad S, Saligheh Rad H. Quantification of human cortical bone bound and free water in vivo with ultrashort echo time MR imaging: a model-based approach. Radiology. 2017; 283:862–872. [PubMed: 28051911]
24. Granke M, Makowski AJ, Uppuganti S, Does MD, Nyman JS. Identifying novel clinical surrogates to assess human bone fracture toughness. J Bone Miner Res. 2015; 30:1290–1300. [PubMed: 25639628]
25. Jerban S, Ma Y, Li L, et al. Volumetric mapping of bound and pore water as well as collagen protons in cortical bone using 3D ultrashort echo time cones MR imaging techniques. Bone. 2019; 127:120–128. [PubMed: 31176044]
26. Cao H, Ackerman JL, Hrovat MI, Graham L, Glimcher MJ, Wu Y. Quantitative bone matrix density measurement by water- and fat-suppressed proton projection MRI (WASPI) with polymer calibration phantoms. Magn Reson Med. 2008; 60:1433–1443. [PubMed: 19025909]
27. Chen J, Chang EY, Carl M, et al. Measurement of bound and pore water T1 relaxation times in cortical bone using three-dimensional ultrashort echo time cones sequences. Magn Reson Med. 2017; 77:2136–2145. [PubMed: 27263994]
28. Carl M, Bydder GM, Du J. UTE imaging with simultaneous water and fat signal suppression using a time-efficient multispoke inversion recovery pulse sequence. Magn Reson Med. 2016; 76:577–582. [PubMed: 26309221]
29. Li S, Ma L, Chang EY, et al. Effects of inversion time on inversion recovery prepared ultrashort echo time (IR-UTE) imaging of bound and pore water in cortical bone. NMR Biomed. 2015; 28:70–78. [PubMed: 25348196]
30. Gurney PT, Hargreaves BA, Nishimura DG. Design and analysis of a practical 3D cones trajectory. Magn Reson Med. 2006; 55:575–582. [PubMed: 16450366]
31. Du J, Carl M, Bydder M, Takahashi A, Chung CB, Bydder GM. Qualitative and quantitative ultrashort echo time (UTE) imaging of cortical bone. J Magn Reson. 2010; 207:304–311. [PubMed: 20980179]
32. Du J, Sheth V, He Q, et al. Measurement of T1 of the ultrashort T2* components in white matter of the brain at 3T. PLoS One. 2014; 9:e103296. [PubMed: 25093859]
33. Ma YJ, Lu X, Carl M, et al. Accurate T1 mapping of short T2 tissues using a three-dimensional ultrashort echo time cones actual flip angle imaging-variable repetition time (3D UTE-Cones AFI-VTR) method. Magn Reson Med. 2018; 80:598–608. [PubMed: 29314235]
34. Li C, Seifert AC, Rad HS, et al. Cortical bone water concentration: dependence of MR imaging measures on age and pore volume fraction. Radiology. 2014; 272:796–806. [PubMed: 24814179]
35. Manhard MK, Horch RA, Harkins KD, Gochberg DF, Nyman JS, Does MD. Validation of quantitative bound- and pore-water imaging in cortical bone. Magn Reson Med. 2014; 71:2166–2171. [PubMed: 23878027]
36. Marcon M, Keller D, Wurnig MC, et al. Separation of collagen-bound and porous bone-water longitudinal relaxation in mice using a segmented inversion recovery zero-echo-time sequence. Magn Reson Med. 2017; 77:1909–1915. [PubMed: 27221236]
37. Seifert AC, Wehrli SL, Wehrli FW. Bi-component T2 * analysis of bound and pore bone water fractions fails at high field strengths. NMR Biomed. 2015; 28:861–872. [PubMed: 25981785]
38. Fantazzini P, Brown RJ, Borgia GC. Bone tissue and porous media: common features and differences studied by NMR relaxation. Magn Reson Imaging. 2003; 21:227–234. [PubMed: 12850712]

39. Jerban S, Ma Y, Wong JH, et al. Ultrashort echo time magnetic resonance imaging (UTE-MRI) of cortical bone correlates well with histomorphometric assessment of bone microstructure. Bone. 2019; 123:8–17. [PubMed: 30877070]
40. Han M, Rieke V, Scott SJ, et al. Quantifying temperature-dependent T1 changes in cortical bone using ultrashort echo-time MRI. Magn Reson Med. 2015; 74:1548–1555. [PubMed: 26390357]
41. Kleinberg RL, Farooqui SA. T1/T2 ratio and frequency dependence of NMR relaxation in porous sedimentary rocks. J Colloid Interface Sci. 1993; 158:195–198.
42. Horch RA, Nyman JS, Gochberg DF, Dortch RD, Does MD. Characterization of 1H NMR signal in human cortical bone for magnetic resonance imaging. Magn Reson Med. 2010; 64:680–687. [PubMed: 20806375]
43. Biswas R, Bae W, Diaz E, et al. Ultrashort echo time (UTE) imaging with bi-component analysis: bound and free water evaluation of bovine cortical bone subject to sequential drying. Bone. 2012; 50:749–755. [PubMed: 22178540]
44. Harkins K, Uppuganti S, Nyman J, Does M. Robust pore water suppression in cortical bone with multiple adiabatic inversion recovery. In: Proceedings of the 25th annual meeting of ISMRM, Hawaii, USA 2017, P1588.
45. Ma YJ, Zhu Y, Lu X, Carl M, Chang EY, Du J. Short T2 imaging using a 3D double adiabatic inversion recovery prepared ultrashort echo time cones (3D DIR-UTE-Cones) sequence. Magn Reson Med. 2018; 79:2555–2563. [PubMed: 28913879]

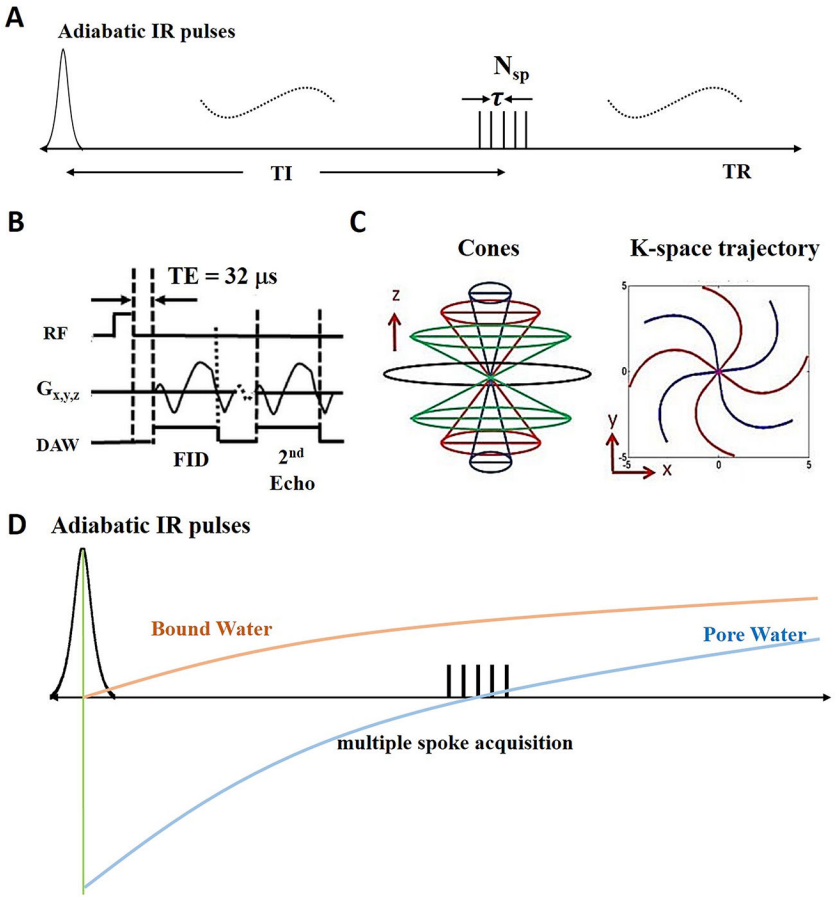

Figure 1.

The 3D IR-UTE-Cones sequence employs an adiabatic inversion pulse for long T_2 suppression, followed by Cones data acquisition with multiple spoke sampling (A). In the basic 3D UTE-Cones sequence, a short rectangular pulse is used for signal excitation followed by 3D spiral sampling with a minimal nominal TE of 32 μs and a second echo with a TE of 2.5 ms (B). The spiral trajectories are arranged with conical view ordering (C). The longitudinal magnetization of pore water in cortical bone is almost completely inverted by the adiabatic IR pulse, while that of bound water is mostly saturated due to its extremely short T_2 (D). TI is selected to null the pore water signal. During TI, the bound water longitudinal magnetization recovers and is selectively detected by the subsequent UTE data acquisition.

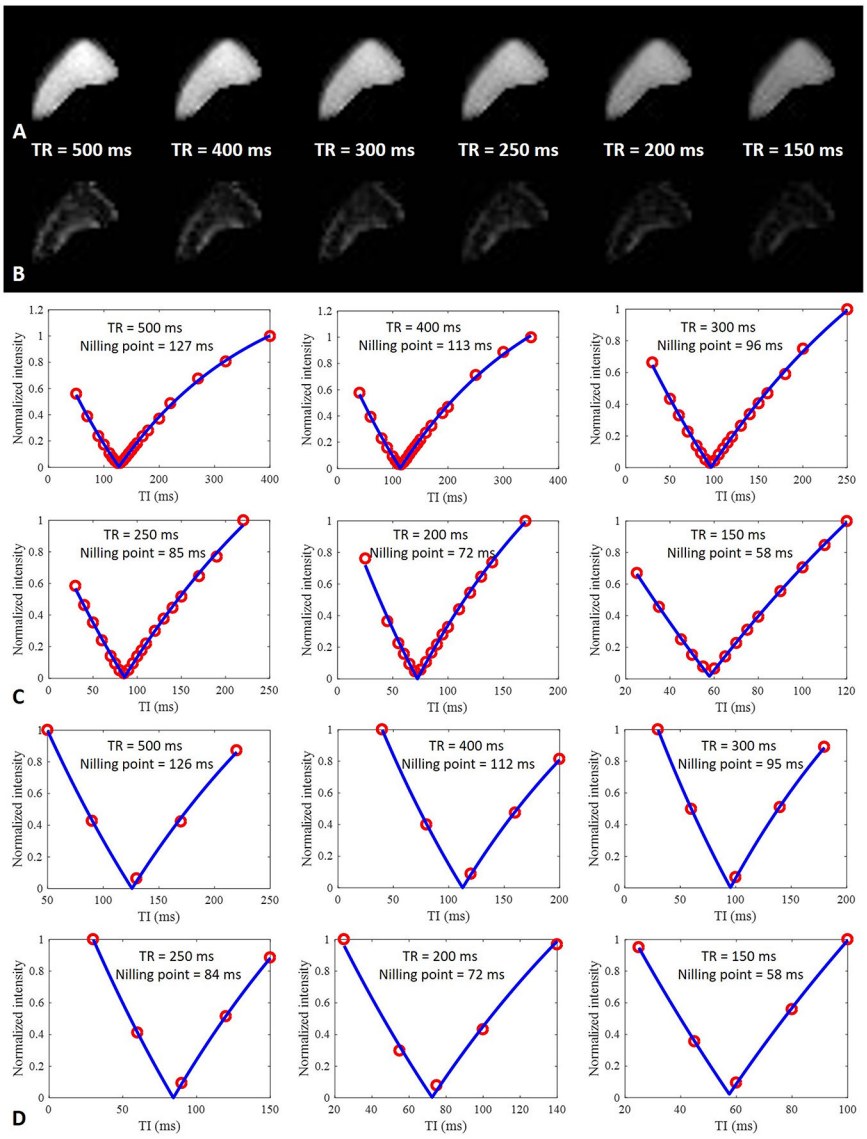

Figure 2.

Representative dual-echo 3D IR-UTE Cones images of a tibial midshaft cortical bone sample from a 38-year-old donor with a TE of 32 μs (A) and 2.5 ms (B) at the nulling point for each TR, and fitting of the TI data using the complete set of TIs (C) and five TIs (D) to determine the optimal nulling point at each TR. Pure bound water images were generated using the calculated nulling points which completely suppressed signal from pore water. The signal intensity of bound water decreased with the use of shorter TRs (A). The images acquired with a TE of 2.5 ms at the nulling point of pore water at each TR show near zero signal level, consistent with complete suppression of pore water signal (B). Comparison of multiple TI fitting (C) with five TIs fitting (D), shows that the calculated nulling points for each TR are nearly identical, suggesting that the faster protocol can be used for accurate estimation of pore water nulling time at each TR.

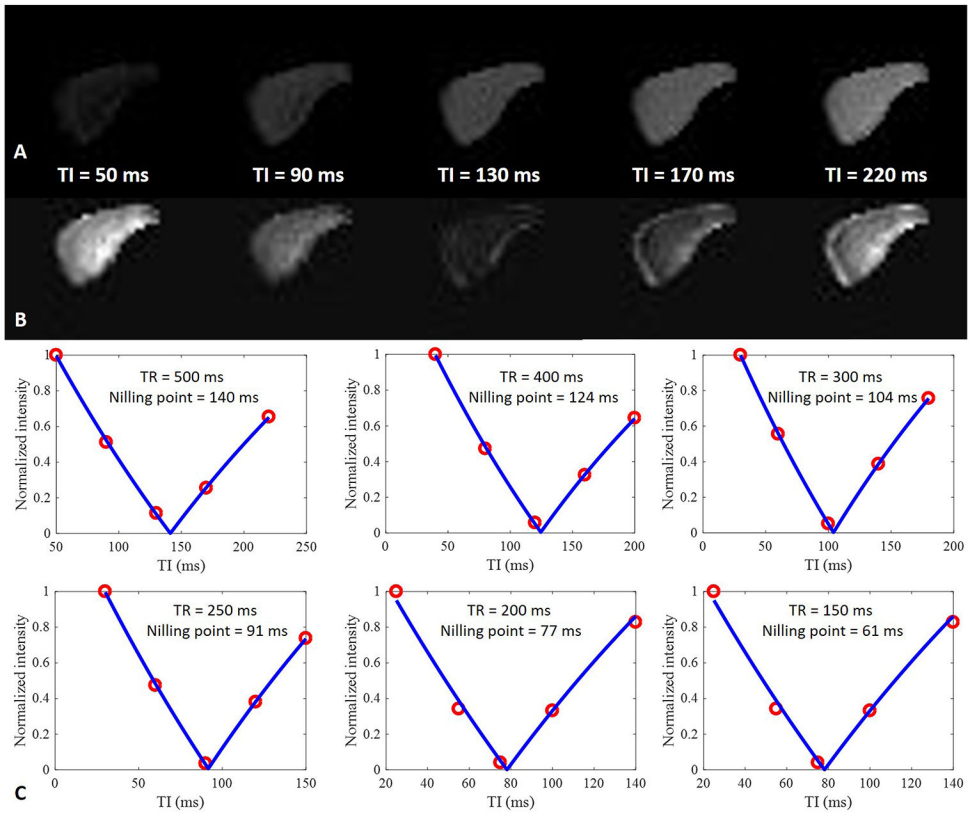

Figure 3.

A cortical bone sample from a 90-year-old donor imaged with a dual-echo 3D IR-UTE Cones sequence with a TR of 500 ms, and a TE of 32 μs (A) and 2.5 ms (B). Signal intensity for the first echo increases with TI from 50 to 220 ms (A), while signal intensity for the second echo decreases with TI until a minimum signal intensity is reached at a TI of 130 ms; it then increases with TI (B). Excellent curve fitting was achieved for IR-UTE signal intensities of the second echo at five TIs, allowing accurate estimation of pore water nulling times which were 140, 124, 104, 91, 77, and 61 ms for TRs of 500, 400, 300, 250, 200 and 150 ms, respectively (C).

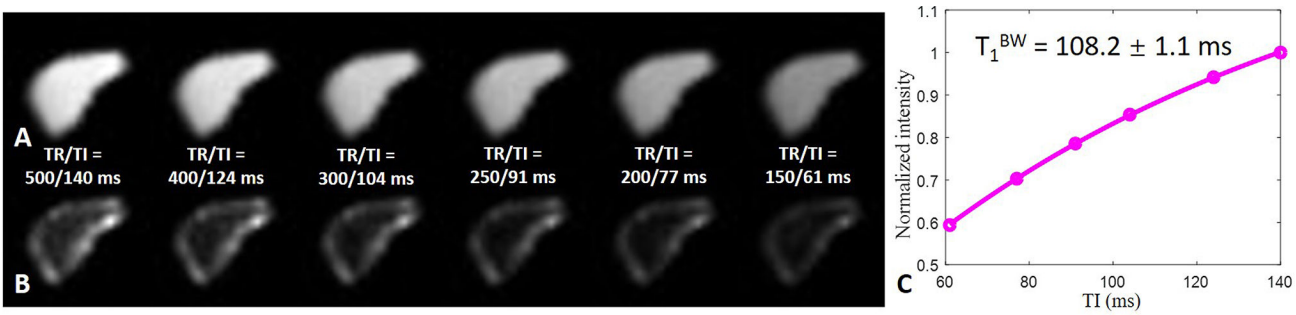

Figure 4.

Representative bound (A) and pore (B) water images of the same cortical bone sample shown in Figure 3 acquired with 3D dual-echo IR-UTE Cones using the calculated nulling points at six TRs from 500 to 150 ms, respectively, and the corresponding T_1^{BW} estimation (C). A T_1 of 108.2 ± 1.1 ms was demonstrated for bound water in this bone specimen.

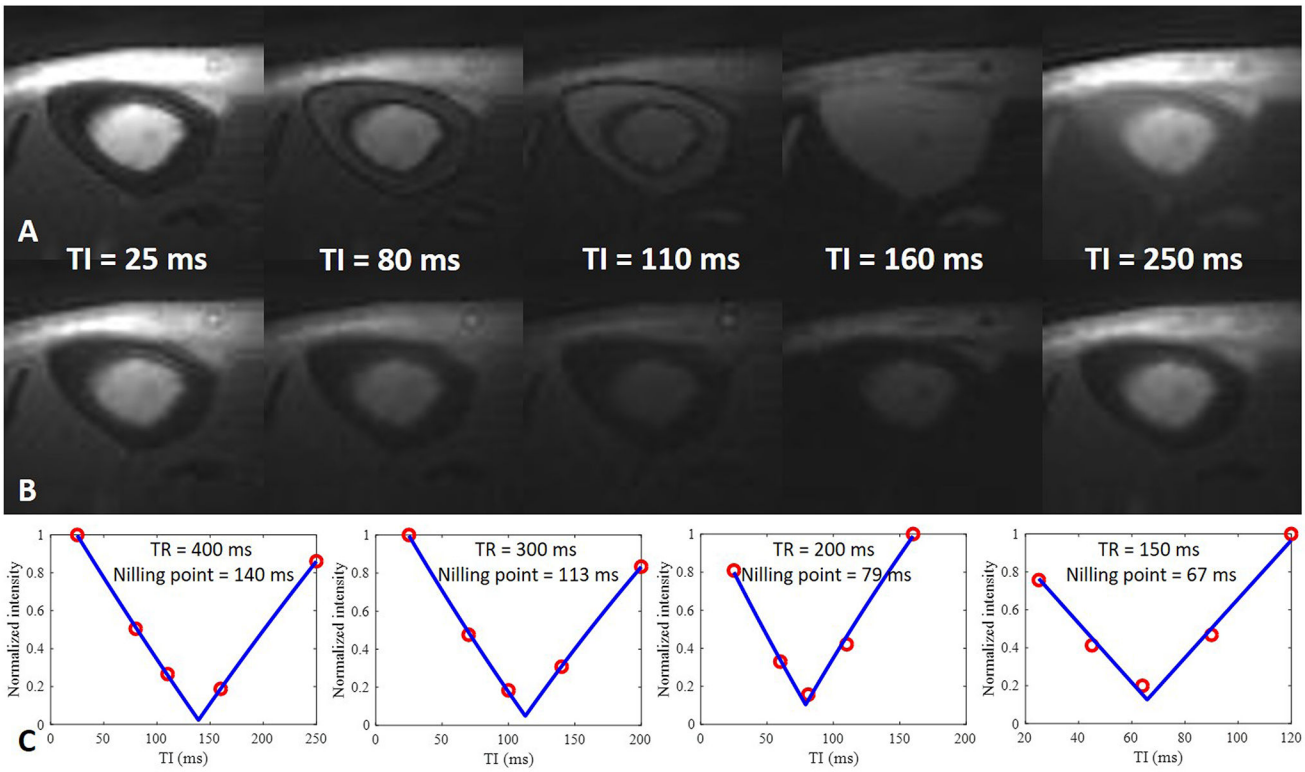

Figure 5.

The tibial mid-shaft of a 34-year-old male volunteer imaged with dual-echo 3D IR-UTE Cones with a TR of 400 ms, TEs of 32 μs (A) and 2.5 ms (B), and five TIs of 25, 80, 110, 160, 250 ms, respectively. Excellent curve fittings were achieved between IR-UTE signal intensities of the second echo and five TIs, allowing accurate estimation of pore water nulling times of 140, 113, 79, and 67 ms for TRs from 400 to 150 ms, respectively (C).

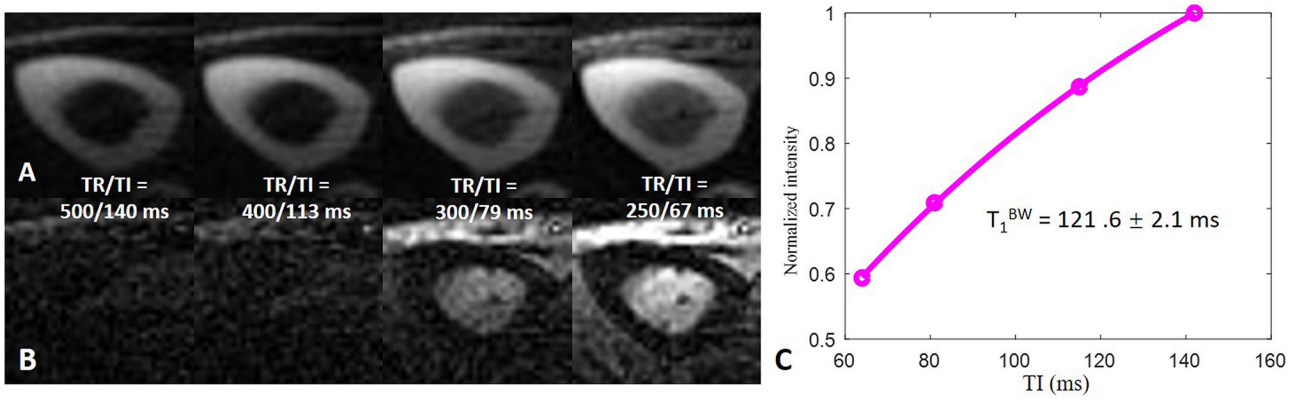

Figure 6.

Representative bound (A) and pore (B) water images of the tibial mid-shaft of the same volunteer in Figure 5 acquired with dual-echo 3D IR-UTE Cones using the calculated nulling points for the four TRs respectively, and the corresponding T_1^{BW} estimation (C). A short T_1 of 121.6 ± 2.1 ms was demonstrated for bound water in the tibial midshaft of this volunteer.

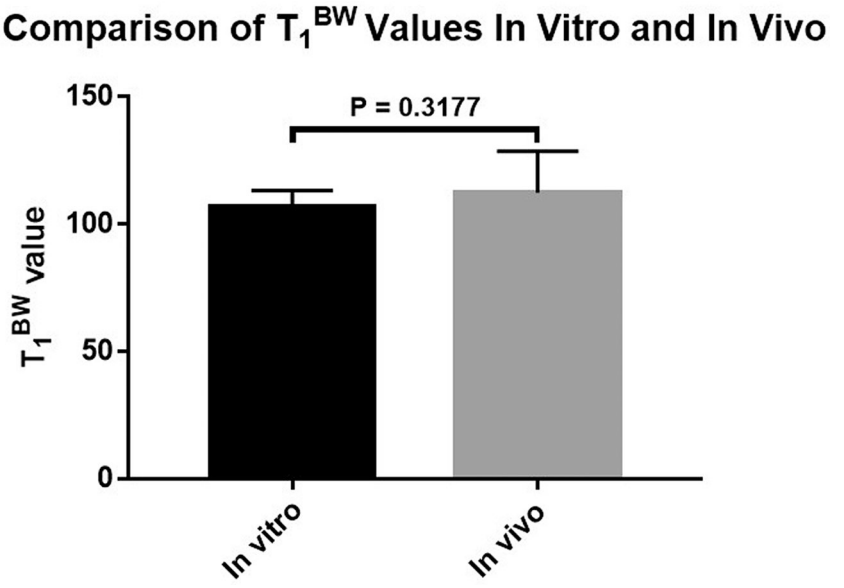

Figure 7.

The mean cortical bone T_1^{BW} of in vitro and in vivo groups were 106.9 ± 6.3 ms and 112.3 ± 16.4 ms, respectively. No significant difference was seen between the two groups.

Table 1

Selected TR and TI combinations to calculate pore water nulling points for in vitro and in vivo studies

TR	TI
In vitro study with multiple TIs	
500 ms	50, 70, 90, 100, 110, 115, 120, 125, 130, 135, 140, 145, 150, 155, 160, 170, 180, 200, 220, 270, 320, 400 ms
400 ms	40, 60, 80, 90, 100, 105, 110, 115, 120, 125, 130, 135, 140, 145, 150, 160, 170, 190, 200, 250, 300, 350 ms
300 ms	30, 50, 60, 70, 80, 85, 90, 95, 100, 105, 110, 115, 120, 130, 140, 150, 160, 180, 200, 250 ms
250 ms	30, 40, 50, 60, 70, 75, 80, 85, 90, 95, 100, 105, 110, 120, 130, 140, 150, 170, 190, 220 ms
200 ms	25, 45, 55, 60, 65, 70, 75, 80, 85, 90, 95, 100, 110, 120, 130, 140, 170 ms
150 ms	25, 35, 45, 50, 55, 60, 65, 70, 75, 80, 90, 100, 110, 120 ms
In vitro study with five TIs	
500 ms	50, 90, 130, 170, 220 ms
400 ms	40, 80, 120, 160, 200 ms
300 ms	30, 60, 100, 140, 180 ms
250 ms	30, 60, 90, 120, 150 ms
200 ms	25, 55, 75, 100, 140 ms
150 ms	25, 45, 60, 80, 100 ms
In vivo study with five TIs	
400 ms	25, 80, 110, 160, 250 ms
300 ms	25, 70, 100, 140, 200 ms
200 ms	25, 60, 81, 110, 160 ms
150 ms	25, 45, 64, 90, 120 ms
Note: TR = repetition time, TI = inversion time	

Note: TR = repetition time, TI = inversion time

Table 2

Determination of nulling points by fitting IR-UTE data with multiple TIs and with five TIs.

TR (ms)	Nulling point fitting with multiple TIs (ms)	Nulling point fitting with five TIs	ICC	P value
500	142.1 ± 12.0	141.3 ± 11.6	0.999 (0.998, 1.000)	< 0.001
400	123.8 ± 8.6	123.4 ± 8.9	0.998 (0.994, 0.999)	< 0.001
300	102.4 ± 5.9	101.3 ± 6.2	0.993 (0.974, 0.998)	< 0.001
250	89.8 ± 5.2	88.9 ± 5.3	0.993 (0.977, 0.998)	< 0.001
200	74.8 ± 4.2	74.8 ± 4.2	0.992 (0.973, 0.998)	< 0.001
150	59.3 ± 3.7	59.2 ± 3.9	0.999 (0.995, 1.000)	< 0.001

Note: Data in means ± standard deviation. Data in parentheses are the 95% confidence interval.

$P < 0.05$ indicates a significant difference.

ICC = intraclass correlation coefficient, TI = inversion time, TR = time of repetition.